PART II

Long Period Waves, Storm Surges and Wave Groups

CHAPTER 57

THE GENERATION OF LOW-FREQUENCY WAVES BY A SINGLE WAVE GROUP INCIDENT ON A BEACH

G. Watson [1] T.C.D. Barnes [2] and D.H. Peregrine [3]

Abstract

The generation of a single low-frequency wave (LFW) pulse by a single group of waves incident on a beach is investigated by means of laboratory experiments and a numerical model. This simplified case allows the LFW to be measured in isolation, after the incident group has passed and before there is any reflection from the wavemaker. A beach consisting of two different slopes (1:100 and 1:20) was used, and runs were made with the water level on each slope. The results were simulated using a composite numerical model, with Boussinesq equations in the deeper water and nonlinear shallow water equations in the surf zone. For some calculations, a friction term was included. For the 1:20 slope, the outgoing LFW is well predicted even without the friction term. With a 1:100 slope, a friction factor of 0.01 gave a good result, in this case reducing the amplitude of the outgoing LFW by a factor of about 2 compared with the frictionless result. The nondimensional equations show that the friction term is insignificant if the beach slope is large compared with the friction factor. Runs of the surf zone part of the model show the outgoing LFW to be correlated with the swash motion. Its amplitude is largest if the duration of the wave group is similar to the swash period of the largest wave in the group. The model also showed a slightly stronger than linear dependence of LFW amplitude on incident wave amplitude.

[1]Research Associate, University of Bristol, Mathematics Department, University Walk, Bristol BS8 1TW, United Kingdom. *Current address:* Disaster Prevention Research Institute, Kyoto University, Gokasho, Uji, Kyoto 611, Japan. (*gary.watson@bristol.ac.uk*)

[2]Research Assistant, University of Bristol. (*tim.barnes@bristol.ac.uk*)

[3]Professor of Applied Mathematics, University of Bristol. (*d.h.peregrine@bristol.ac.uk*)

1. Introduction

Low-frequency waves (LFW) with periods typically 5 to 15 times those of wind-generated waves are formed when wind waves meet beaches. Hamm, Madsen & Peregrine (1993) give a general review of the phenomenon, whilst Herbers et al. (1992) give a good review of recent field measurements. Recent work on the theory of LFW generation has been published by Cox et al. (1992), List (1992a,b), Roelvink et al. (1992), Roelvink (1993) and Schäffer (1993). Low-frequency swash oscillations, with bichromatic waves, have also been investigated by Mase (1994).

In this work, our aim was to throw some light on the question of how such waves are generated, by investigating the simplest possible case of LFW generation in as much detail as possible. Watson & Peregrine (1992) investigated the generation of low-frequency waves in the surf zone using a numerical model based on the nonlinear shallow-water equations. A single group of waves was used to illustrate the process whereby a group forces a variable set-up near the shoreline, which then travels offshore as a single LF pulse. This process has now been investigated more quantitatively, by means of laboratory experiments and a wider range of numerical computations. The range of validity of the model has also been extended by coupling the surf zone model to a Boussinesq model in the deeper water.

The reason for choosing a single group of waves rather than continuous bichromatic waves (such as those used by Kostense, 1984) was that this allows the outgoing LFW to be measured in isolation. By the time it reaches the deeper water, the incident wave group has already passed by. It is also measured before reflecting off the paddle. With continuous waves such reflections will contaminate the results unless they are mechanically removed or taken into account in the data analysis. Both of these are difficult to achieve with any degree of confidence.

Details of the experiments, and discussion of one run showing the generation of an outgoing LF pulse, are given in Section 2. A more detailed account of the experiments will be available in the Ph.D. thesis of T. Barnes. The numerical model is described briefly in Section 3 and its results are compared with the measurements, showing the importance of friction effects on the shallower beach slope. Section 4 discusses the influence of friction in more detail. Section 5 illustrates the correlation between swash motions and the outgoing LFW, using results from various other runs of the surf zone part of the model. The importance of the relative timescales of group period and swash period is pointed out. Discussion and conclusions are given in Section 6.

2. Experimental Results

Description of Experiments

Experiments were performed in a 50 m long wave flume at Hydraulics

Research Ltd. in Wallingford, England. The flume is 1 m wide. It is equipped with a piston-type wavemaker with two paddles, controlled by a PC. A concrete beach with two slopes, 1:100 and 1:20, was installed in the flume as shown in Figure 1. Runs were performed using two different water depths of 0.35 m and 0.20 m, so that the undisturbed shoreline would lie on a different slope in each case.

An array of resistance-type wave probes was used, and Figure 1 shows their layout for the deeper water runs. Probe 1 was located near the paddle in order to measure the generated wave signal. Probes 2 and 3 were in the deeper water. Probes 4–11 were on the 1:100 slope and Probe 12 was on the 1:20 slope.

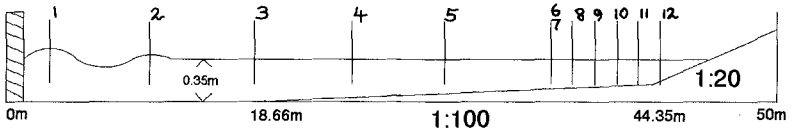

Figure 1: Cross-section of the HR wave flume, showing beach and positions of wave probes (not to scale). A current meter was located at Probe 6.

Since a number of numerical runs were to be performed using just the surf zone model, particular attention was paid to measurements at a point where all but the smallest waves had already broken. In the case illustrated, this was near Probes 6 and 7, (depth 15.5 cm). Two probes were used at this point in order to check for consistency across the tank.

Along-tank velocity data were also collected at this point, using an ultrasonic current meter. The sensor head was placed at about half the water depth, the results having been found not to be very sensitive to the precise placement of the probe. At this location, the incident and outgoing signals are not separated in time, but can be approximately separated by calculating the Riemann invariants. This is done by combining the surface elevation and velocity signals as explained in Section 3.

Wavemaker Signal

Initially, single groups consisting of modulated sine waves were used. However, these waves acquired large second harmonics as they propagated along the tank, with each wave effectively splitting into two. To solve this problem, groups consisting of solitary wave solutions to the Korteweg-deVries equation were used instead. For the shallow water regime of these experiments, this is more appropriate than Stokes theory, which is better in deeper water. Stokes theory requires the Ursell parameter $U = ka_0/(kh)^3$, to be small, whereas in these experiments it was of order 1. In the formula for U, k is the wavenumber, a_0 the fundamental amplitude and h the undisturbed water depth.

The wavemaker signal was designed to produce surface elevation time series of the form

$$\eta = \sum_i \eta_i \mathrm{sech}^2 \sqrt{\frac{3\eta_i}{4h_i^3}} c_i(t - t_i) - (a + a_s)\sin\omega t \qquad 0 \le t \le \pi/\omega \quad (1)$$

and zero outside that time interval. The wave times, t_i, were equally spaced. The wave amplitudes, η_i, were sinusoidally modulated by the function $\eta_i = A\sin\omega t_i$. The water depth for each wave, h_i, must be adjusted for the additional sine function: $h_i = h_0 - (a+a_s)\sin\omega t_i$. The wave speed c_i is $\sqrt{g(h_i + \eta_i)}$. Velocity was estimated from the shallow-water approximation $u = \sqrt{g/h_0}\,\eta$ and then integrated to give the wavemaker displacement signal.

The stroke of the paddle is not great enough to make a succession of solitary waves, each with its own net displacement. For this reason, the sine function was added. This has the same duration as the group and corresponds to a set-down beneath it. This means that there is little net mass flux in the incident wave groups.

Results

Surface elevations from a typical run in the deeper water (1:20 slope) are shown as the thick lines in Figure 2. All of the runs yielded results which were qualitatively similar. Numerical predictions from the model described below are included for comparison. The shape of the initial wave group, consisting of five waves, is seen in the trace from Probe 1. The form of the solitary waves is preserved quite well along the constant depth section, except for the development of a small dispersive tail (1–3). As the wave group travels into shallower water, the waves steepen and at Probe 6/7 all except the first are breaking. Near the shoreline (11 & 12) a LFW is seen to develop consisting of a peak, apparently like wave set-up, followed by a trough. At the same time the short waves dissipate their energy and get smaller, so that the LFW is more prominent. This wave then propagates offshore, decreasing in amplitude as it does so. At Probe 5 it is separated in time from the incident group. Further offshore it can be identified quite clearly. The moving peak and trough are marked with arrows. It then reflects off the wavemaker (also marked). At Probe 1, the amplitude appears to be twice as big, due to the superposition of the reflection.

The shape and amplitude of the outgoing LFW can be seen more clearly if the vertical scale of the plots is expanded. This is shown for Probes 2–5 in Figure 3.

3. Composite Numerical Model

A coupled numerical model, based on the nonlinear shallow-water equations (NLSWE) in the surf zone (Watson and Peregrine, 1992) and the Boussi-

nesq equations in deeper water, is able to simulate the phenomenon.

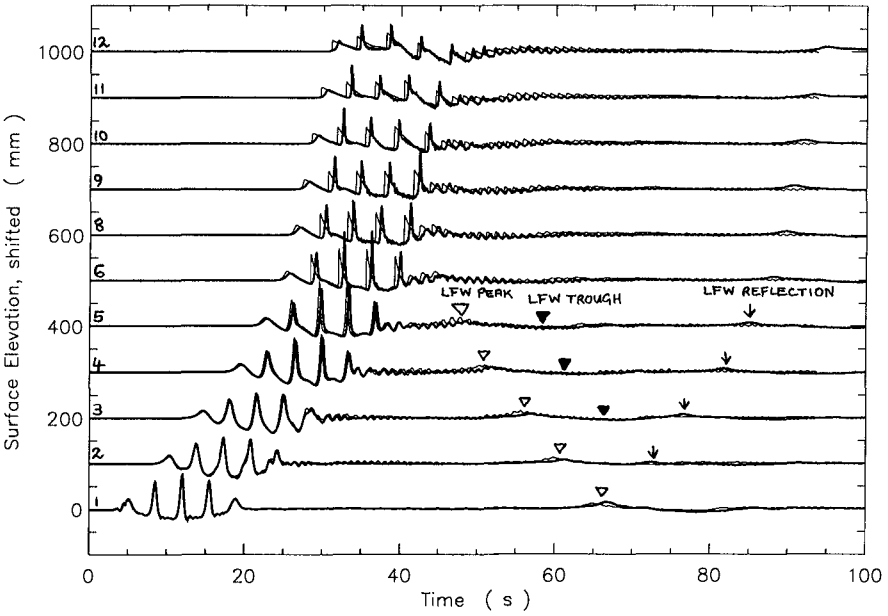

Figure 2: *Thick line:* Surface elevation time series at each probe (except 7) for a group of five solitary waves. *Thin line:* Numerical prediction.

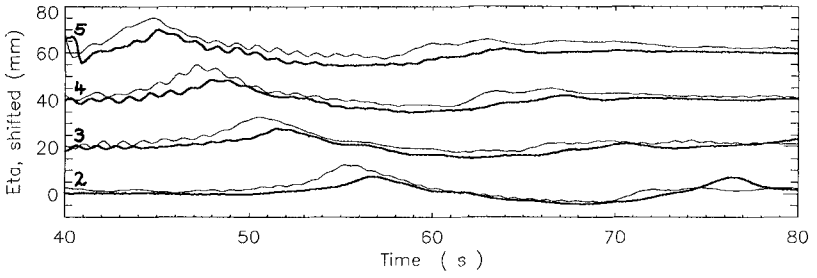

Figure 3: Expanded view of the outgoing LFW in Figure 2, for Probes 2–5. *Thick line:* Measurements. *Thin line:* Numerical prediction.

Our primary interest here is in the mechanisms by which LFW are generated. LFW have their greatest amplitudes in the surf zone, and the most important components of the generation process occur there. It is therefore

important to use a model that includes all the important physics in the surf zone. The nonlinear shallow-water equations for the conservation of mass and momentum, with a friction term, were used:

$$d_t + (ud)_x = 0 \tag{2}$$

$$u_t + uu_x + g\eta_x + \frac{1}{2} f \frac{u \mid u \mid}{d} = 0 \tag{3}$$

where $\eta = d - h$ is the surface elevation, d is the total water depth, h the undisturbed water depth, u the flow velocity, g gravity and f an empirical friction coefficient.

These equations are able to represent spilling breakers as travelling hydraulic jumps or bores, which manifest themselves as discontinuities in the solution. Some information on these equations without the friction term, and the numerical method used to solve them has been given previously (Watson & Peregrine, 1992; Watson, Peregrine & Toro, 1992). Treatment of the moving shoreline boundary condition is discussed in the latter paper.

The friction term in the above equations is the simplest that is conventionally used to represent friction. Typical values for f are of order 10^{-2}. For the present study it was necessary to modify the numerical procedure slightly to allow for this term. This was done by first solving the frictionless equations at timestep n as before, a procedure which is second-order accurate. After this a simple first-order forward difference step was applied at each grid point, altering the velocity u_n by an amount

$$-\frac{1}{2} f \frac{u_n \mid u_n \mid}{d_n} \Delta t \tag{4}$$

Δt must be small enough for this to be reasonably accurate. The inclusion of friction in this manner destroys the second-order accuracy of the scheme. However, since the empirical friction term is rather approximate in any case, the degradation of numerical accuracy here is not important.

In deeper water, the Boussinesq equations are appropriate because they include dispersive terms. The Boussinesq equations in the form due to Peregrine (1967) were used:

$$d_t + (ud)_x = 0 \tag{5}$$

$$u_t + uu_x + g\eta_x = \frac{1}{2} h(hu_t)_{xx} - \frac{1}{6} h^2 u_{xxt} \tag{6}$$

Recently, Dingemans has shown that in some circumstances, particularly on a barred beach, it is important to include further dispersive terms. See Dingemans (1995) for a full discussion. However, in our case it will be seen that the above equations give sufficiently good results. The friction term was not included in these equations, since it becomes small in the deeper water.

The equations were solved numerically using a finite difference scheme due to Peregrine (1967).

Matching the two models together

The models were matched at the join using a characteristics boundary condition. In the frictionless shallow-water equations, the wave signals propagating in each direction are given by the Riemann invariants $R^+ = 2c + u$ and $R^- = 2c - u$, where $c = \sqrt{gd}$ and d is the total water depth. This is also approximately true for the Boussinesq equations, which for waves of sufficiently gentle slope approximate to the shallow-water equations. Thus, an almost non-reflecting join can be made by taking R^+ from the last point of the Boussinesq section and feeding it into the first point of the NLSWE section, and taking R^- from the first point of the NLSWE section and feeding it into the last point of the Boussinesq section.

This being done, a number of runs were made in order to test the sensitivity of results to the position of the join. It was found that the join could be moved a significant distance without much change in the output, as long as it was somewhere in the vicinity of the break point. The run reported here was done with the join at the location of Probe 6 in Figure 1.

The Seaward Boundary Condition

At the offshore end of the computational domain, a boundary condition similar to that at the matching point was applied. This used the characteristic equations to allow outgoing waves to pass out with no reflection. The outgoing R^- was found from data immediately inside the domain, and the surface elevation was forced to be equal to that measured by Probe 1. This was sufficient information to define the incident R^+. Although the reflections from the paddle that were present in the wave flume were not reproduced, these are not of any interest.

Comparison of Numerical and Experimental Results

The numerical results for the data in Figures 2 and 3 are shown as thin lines in those figures. The main feature of interest, i.e. the amplitude, shape and propagation of the outgoing LF pulse, is reasonably well predicted — although the amplitude is a little too large and the timing is not precise. Some properties of the short waves are not reproduced very well as the group travels shoreward. Their amplitude is underpredicted, the sharp wave crest is flattened out, and there are small timing errors. Note however that these details do not appear to have a significant effect on the LFW generation process.

The success of this model in predicting the measured LFW shapes and amplitudes is illustrated in more detail using data from Probe 6. Results from two runs are shown. One has the water level set so that the shoreline is on the 1:20 slope, the other with the shoreline on the 1:100 slope.

In both cases the model was run using the measured water depth and velocity at Probe 6, to construct a time series of the Riemann invariant $R^+ = 2\sqrt{gd} + u$. The outgoing LFW was then examined by computing the other invariant $R^- = 2\sqrt{gd} - u$. This is plotted using dashed lines in Figures 4 and 5 for the two runs, together with the numerical result. Both cases show the LFW quite clearly. There are spikes in the data every time an incident wave passes the probe. This effect is due to the fact that the shallow-water equations on which the Riemann invariant analysis is based do not accurately describe the details of the crests of steep waves, breakers, or bores.

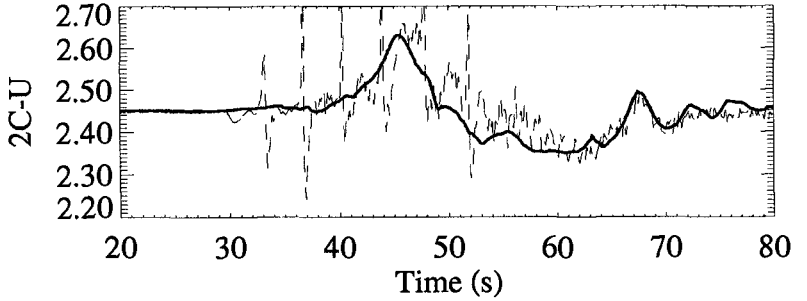

Figure 4: Outgoing signal at seaward boundary in deep water case (composite slope with shoreline on the 1:20 slope). Data (broken), frictionless model (solid).

In the deeper water case (1:20, Figure 4), the agreement between model and data is quite good, except for precise details of the wave shape. In this case, the model gave almost the same result with or without friction. The frictional result is not plotted.

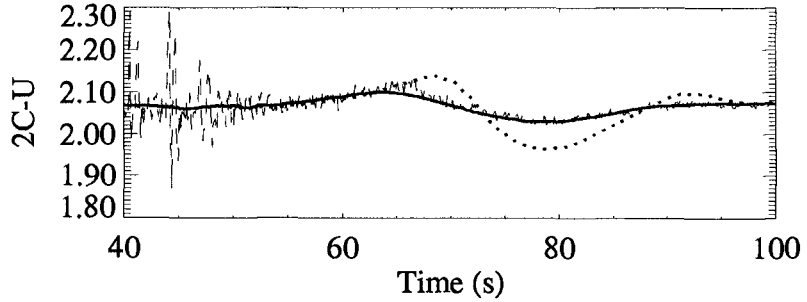

Figure 5: Outgoing signal at seaward boundary in shallow water case (1:100 slope). Data (broken), frictionless model (dotted), frictional model (solid).

In the shallower case (1:100, Figure 5), agreement in the frictionless case is not so good (dotted). The LFW is overpredicted by a factor of about 2. The shape of the pulse is also different, in that the peak occurs about 5 s

late. However when the friction term is included, with the value $f = 0.01$, the result is much better — as shown by the solid curve. The effect of friction is discussed in more detail in the following section.

4. The Effect of Friction

The frictional drag force acting between the bottom and the water has an increasingly strong effect as the depth decreases. This is simply because the friction force is primarily determined by the near-bottom velocity of the water, and in the shallow-water approximation it acts on a mass of water that is proportional to the depth. It will thus have its strongest effect in the swash zone, where the water is shallowest. Since this is where LFW processes are particularly important, it is to be expected that friction may have some effect on LFW generation.

For a plane beach of slope α extending fom the shoreline to the offshore boundary, the relative importance of friction effects may be seen from the following scaling argument. Eqs. 2 & 3 may be written using the following non-dimensional variables:

$$x' = x/x_1, \quad d' = d/h_1, \quad \eta' = \eta/h_1, \quad u' = u/u_1, \quad t' = t/t_1$$

where the scaling variables are x_1 (the distance between the offshore boundary and the undisturbed shoreline), h_1 (the undisturbed water depth at the offshore boundary), $u_1 = \sqrt{gh_1}$ and $t_1 = x_1/u_1$. Dropping primes, the equations become:

$$d_t + (ud)_x = 0 \tag{7}$$

$$u_t + uu_x + \eta_x + \frac{1}{2}\frac{f}{\alpha}\frac{u|u|}{d} = 0 \tag{8}$$

where α is the slope h_1/x_1.

For breaking waves, u^2/d is of order 1, so the friction term is of order f/α. Thus friction can be expected to have a negligible effect if $f \ll \alpha$, a noticeable effect if $f \sim \alpha$ and to dominate everywhere if $f \gg \alpha$. In the two cases under consideration, with $f = 0.01$, f/α takes the values 0.2 and 1.0. In the former case friction had little effect, whereas in the latter the outgoing LFW amplitude was reduced by a factor of about 2.

These conclusions were further confirmed by model runs made using a range of values of f. The same incident wave group as in Watson & Peregrine (1992) was used, and the height of the outgoing LF pulse was determined by taking the difference between maximum and minimum in R^- at the offshore boundary. Six runs with values of f/α ranging from 0.0 to 2.0 were performed. The results are plotted in Figure 6.

The figure shows a strong dependence of outgoing LFW amplitude on the scaled friction factor f/α. With no friction ($f/\alpha = 0$), the amplitude has its maximum value, but this is reduced quite rapidly as f/α is increased, so

that for $f/\alpha = 0.2$ the LFW amplitude is 78% of its maximum value. As f/α is increased, the amplitude continues to decrease, although more slowly. for $f/\alpha = 1.0$, it is 47% of its maximum value. This is roughly consistent with the results in Figures 4 and 5.

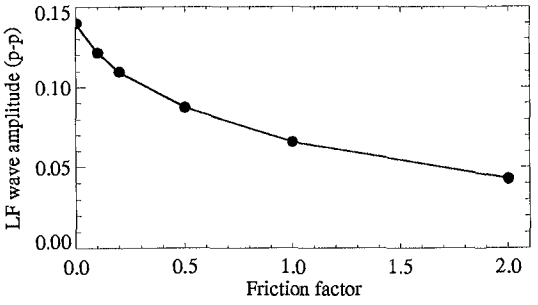

Figure 6: The dependence of outgoing LFW amplitude on scaled friction factor, f/α.

This means that the agreement which was obtained in the 1:100 case with $f = 0.01$ is open to the suggestion that it may have been merely coincidental. However, this value was chosen from experience as being one that is typically used.

5. The Importance of Swash Motions

During the time that the wave group is in the swash zone, there is a complex interaction between the waves in the group and the swash motion from previous waves. This affects the amplitude and shape of the LFW that finally emerges. The nature of the swash, and the properties of the LFW, depend on the relative values of the various timescales in the problem. Rather than attempt to understand the swash motion in detail, this effect was investigated in a more empirical manner by performing a number of runs of the model with different timescales and hence different swash regimes.

The timing of the incident group is determined by two parameters: the wave period, τ, and the number of waves in the group, N. The total duration of the group is then $T = N\tau$. There is a third timescale in the problem, namely the natural period of swash on the beach. Let us call this t_s. This depends on the amplitude of the incident waves. In the frictionless case (considered here), the swash motion approximates fairly closely to free motion under gravity on the sloping beach. Thus, the larger the incident waves, the greater the initial velocity of the uprush and the longer the swash period t_s.

A number of runs of the model were performed with different wave periods, different numbers of waves and and different swash periods. These were based on variations about a control case, summarized in Figure 7.

The top panel of this figure shows a perspective view of the space-time plot of surface elevation. The input is an idealized group of five sinusoidally modulated sawtooth-shaped waves, which are intended to represent waves that are already breaking. The peak and trough values have been set so that there is no net mass flux in each wave. The curved wave trajectories show how each wave slows down as it approaches the shore, and the wave heights can be seen to diminish in the process. The wave group can be seen to force a mass of water up the beach face on the timescale of the wave group. The seaward-propagating LFW pulse that this forcing generates is just about visible to the right of the wave group in the plot.

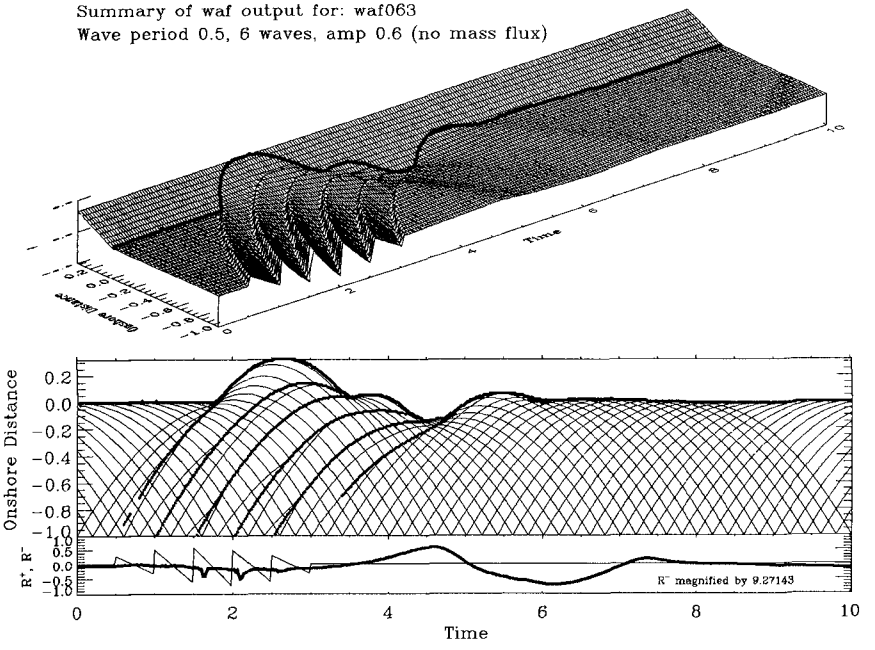

Figure 7: Result from the control case (see text).

The next panel shows shallow-water equation characteristics and bore trajectories (indicated by black dots). The shoreline motion is also shown in plan view. Beneath this, the incident and outgoing signals at the seaward boundary of the model are plotted. These are computed from the Riemann invariants R^+ and R^- as explained in Section 3. Note that the outgoing signal, which shows the shape of the LFW pulse, has been magnified by the indicated factor in order to make it more clearly visible. In this case it is about 10 times

smaller than the incident signal. The main thing to notice from this plot is that the shape of the LFW pulse is very similar to the shape of the runup, especially after the runup has been averaged over the short-wave oscillations.

The generality of this observation was tested by performing a variety of model runs with different timescales. These were then used to investigate the effect of wave group timing on the LFW amplitude. Runs were performed with a range of values of τ and then with a range of values of N, varying the wave group duration T in two different ways. Both sets span approximately the same range of T-values for each wave amplitude, with t_s roughly central in each case. The runs were repeated with two different amplitudes for the largest wave in each group: 0.1 and 0.6 in dimensionless units. This provided two different values of the swash period. Separate runs using just one incident bore showed that for a wave of height 0.1 above still water level, the swash period was $t_s = 1.4$; whereas for a height of 0.6 it was $t_s = 2.9$.

The results of these runs are summarised in Figure 8, with runup plotted next to the LFW signal (at the offshore boundary) for each run. These curves have been smoothed a little to remove discretization effects in the runup, and spikes (due to incident bores) in the LFW signals. Note the clear correlation between the shapes of each pair of signals, with the LFW signal occurring somewhat later than the runup signal. It is significant that this is true despite the runup signals being quite varied in nature.

The runup is plotted so that whatever the range, the vertical extent of the plot is the same. The LFW plots all have the same relative scaling. Ratios of LFW elevation amplitude to incident wave amplitude were in the range 0.015–0.07 (a factor of 4.7). However, ratios of LFW elevation amplitude to runup amplitude were in the narrower range 0.035–0.125 (a factor of 3.6).

These two observations indicate the reflected LFW is better correleted with runup than with the incident wave envelope. This is consistent with the idea that the time-varying set-up within the wave group is manifested as swash when it is near the shore, and then propagates offshore as the outgoing LFW.

The amplitude of the outgoing LFW was found to depend in a consistent way on the relative values of wave group duration T and swash period t_s . This is shown in Figure 9. Here the LFW height, defined as the difference between the maximum and minimum in the LFW pulse, is plotted against T for each run. Four sets of results are presented. Figure 9(a) contains the results for amplitude 0.1, and Figure 9(b) for amplitude 0.6. The thick lines are runs with variable N, and the thin lines for runs with variable τ.

The main feature to note is that each of these curves has a maximum close to the swash period for a single wave of the respective amplitude. This period, t_s, is marked with an arrow on each plot. There are notable differences between the variable-N and variable-τ series, and at present the explanation for this is not clear. However, it is suggested that the presence of a peak in each curve can be explained as a quasi-resonance between the wave group forcing

and the natural swash motion of the water on the beach face. If the wave group period is similar to the swash period ($T \approx t_s$), then a sequence of waves can carry water up the beach following, reinforcing and being carried by the initial swash motion. Thus, a large (wave-averaged) swash motion develops.

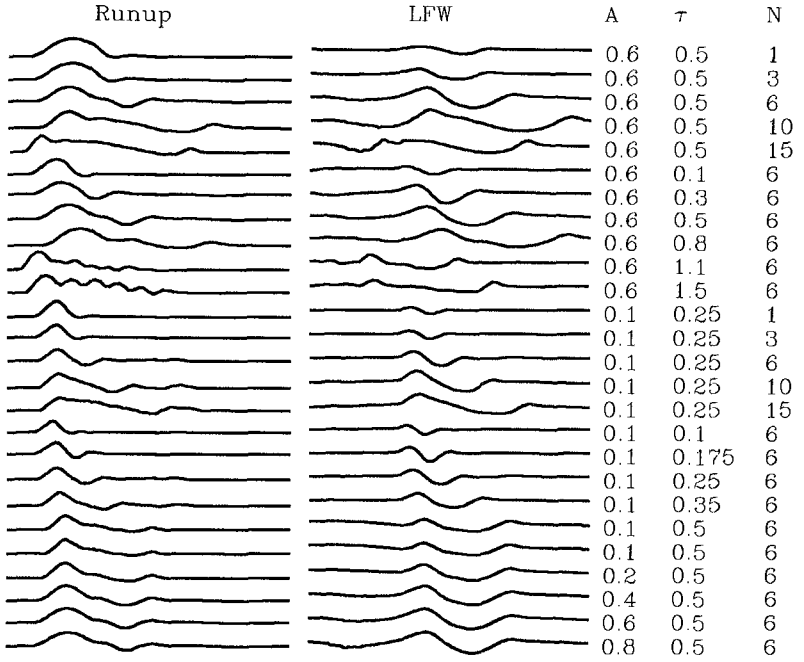

Figure 8: Swash motion and LFW signal for various runs of the model.

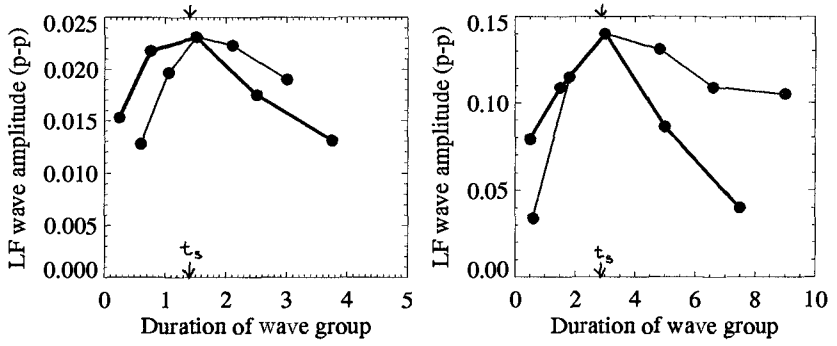

Figure 9: Dependence of LFW amplitude on wave group period T. (a) Amplitude 0.1. (b)Amplitude 0.6.

If the wave group period is longer than this swash period ($T \gg t_s$), then succeeding waves tend to meet swash already coming down the beach, and this opposing effect restricts the development of a large swash. In the extreme case of uniform waves, the swash zone becomes very narrow. For $T \ll t_s$, there is a strong fall-off of LFW amplitude as T decreases. Figure 8 shows that in these cases, the period of the LF motion does not decrease beyond t_s. These shorter groups have less momentum and energy, so can drive less and less fluid up the beach as T decreases.

With continuously modulated waves, rather than a single group, the number of wave groups or fraction of a wave group that is within the surf zone at any one time is expected to be relevant. This may be represented by a group-based surf-similarity parameter, $G = T/t_b$, where T is the duration of the group and t_b is the time it takes the largest wave to reach the shore after breaking. G is small for a wide surf zone and large for a narrow one. If G is small, several groups may simultaneously be generating LFW. There will then be substantial interference, which is likely to be destructive. If it is large, there will only be one or two waves in the surf zone at once: little interaction can occur and LFW generation is expected to be minimal. The strongest LFW generation is expected to occur when G is of order one. This idea remains to be investigated more thoroughly.

6. Discussion and Conclusions

The experiments clearly show the generation of LFW, and the numerical modelling successfully predicts their form and amplitude, even though the finer details of wave breaking are not included. It is clear that friction is important on the gentler slopes, on a laboratory scale, and reduces LFW amplitudes.

In interpreting the numerical and laboratory experiments it appears that the swash zone, and in particular the period of swash from the largest wave of a group, is an important feature. It is not entirely clear however, whether this is an indication of set-up generated in the approach to the shore line or a process centred close to and in the swash zone. In addition, for the practical case where there may be continuous wave modulation we suggest a group surf-similarity parameter based on the size of the surf zone relative to individual groups should be important.

The numerical experiments also indicate a slightly stronger than linear dependence of LFW amplitude on incident wave amplitude, in accord with field observations (Herbers et al., 1992). However, the question as to what LFW are incident on the surf zone, has yet to be resolved. The behaviour of wave groups with differing set-down has been investigated, but is not reported here. The development and decoupling of incident bound waves, as they enter shallow water where the Stokes theory becomes invalid and wave crests behave more like individual solitary waves needs to be determined. This is currently under investigation using a fully nonlinear potential flow solver.

Acknowledgements

This work was funded by the Commission of the European Communities, DG XII, under Contract No. MAS2-CT92-0027 (MAST-II G8-M Coastal Morphodynamics). The authors are grateful to the staff of HR Wallingford for providing facilities and support for the experiments. T. Barnes was funded by an EPSRC CASE research studentship with HR Wallingford. Dr. E.F. Toro of Cranfield Institute of Technology provided the core of the numerical algorithm used for solving the nonlinear shallow water equations.

References

Cox, D.T., N. Kobayashi and A. Wurjanto (1992). Irregular wave transformation processes in surf and swash zones. *Proc. 23rd Int. Conf. Coastal Eng.*, 156–169.

Dingemans, M.W. (1995). *Water wave propagation over uneven bottoms.* World Scientific, in press.

Hamm, L., P.A. Madsen and D.H. Peregrine (1993). Wave transformation in the nearshore zone: a review. *Coastal Eng.*, **21**, 5–39.

Herbers, T.H.C., S. Elgar, R.T. Guza & W.C. O'Reilly (1992). Infragravity-frequency (0.005–0.05 Hz) motions on the shelf. *Proc. 23rd Int. Conf. Coastal Eng.*, 846–859.

Kostense, J.K. (1984). Measurements of surf beat and set-down beneath wave groups. *Proc. 19th Int. Conf. Coastal Eng.*, 724–740.

List, J.H. (1992a). Breakpoint-forced and bound long waves in the nearshore: a model comparison. *Proc. 23rd Int. Conf. Coastal Eng.*, 860–873.

List, J.H. (1992b). A model for two-dimensional surf beat. *J. Geophys. Res.*, **97**, 5623–5635.

Mase, H. (1994). Uprush-backrush interaction dominated and long wave dominated swash oscillations. *Proc. Int. Symp.: Waves — Physical and Numerical Modelling*, UBC Vancouver, August 21–24 1994, eds. M. Isaacson and M. Quirk, 316–325.

Peregrine, D.H. (1967). Long waves on a beach. *J. Fluid Mech.* **27**, 815–827.

Roelvink, J.A., H.A.H. Petit and J.K. Kostense (1992). Verification of a one-dimensional surf-beat model against laboratory data. *Proc. 23rd Int. Conf. Coastal Eng.*, 960–973.

Roelvink, J.A. (1993). Surf beat and its effect on cross-shore profiles. *Ph.D. Thesis*, Technical University of Delft, 116 pp.

Schäffer, H.A. (1993). Infragravity waves induced by short-wave groups. *J. Fluid Mech.* **247**, 551–588.

Watson, G. and Peregrine, D.H. (1992). Low frequency waves in the surf zone, *Proc. 23rd Int. Conf. Coastal Eng.*, 818–831.

Watson, G., Peregrine, D.H. and Toro, E.F. (1992). Numerical solution of the shallow-water equations on a beach using the weighted average flux method. In *Computational Fluid Dynamics '92*, Volume 1, C. Hirsch et al. (Eds.), 495–502.